Article

Emergent collective alignment gives competitive advantage to longer cells during range expansion

Nathan van den Berg[1†], Kristian Thijssen[1†], Thu Trang Nguyen[1†], Adrien Sarlet[1†], Mireia Cordero[1], Alba García Vázquez[1], Namiko Mitarai[1], Amin Doostmohammadi[1], and Liselotte Jauffred[1]

[1]The Niels Bohr Institute, University of Copenhagen, Blegdamsvej 17, DK-2100 Copenhagen O, Denmark
[†]These authors contributed equally
[1]Correspondence: mitarai@nbi.ku.dk, doostmohammadi@nbi.ku.dk, jauffred@nbi.ku.dk

Keywords: Biofilm, morphology, Escherichia coli, range expansion, spatio-genetic patterning, 3D growth

ABSTRACT Bacteria's competition for nutrients and territory drives biofilm evolution (1–4). The factors determining the outcome of competition among diverse bacterial species have a broad impact on a wide range of pathological (5), environmental (6), and microbiome interactions (7). While motility-related traits (8–11) and specific molecular mechanisms (12, 13) have been identified as potential winning attributes in bacteria, a shared and universally conserved feature determining competition remains elusive. Here, we demonstrate that a simple morphological feature of individual bacteria, cell aspect ratio, provides a winning trait for the population. Using growth-based range expansion experiments (14), we show that relatively longer bacteria robustly conquer the expanding front, even when initially in minority. Using an agent-based model of dividing bacteria, we reveal that the takeover mechanism is their emergent collective alignment: groups of locally aligned bacteria form "nematic arms" bridging the central region of the colony to the expanding front. Once at the front, bacteria align parallel to it and block the access of shorter bacteria to nutrients and space. We confirm this observation with single-cell experiments and further generalise our findings by introducing a generic continuum model of alignment-dominated competition, explaining both experimental and cell-based model observations. Moreover, we extend our predictions to spherical range expansions (15) and confirm the competitive advantage of being longer, even though the effect is less pronounced than in surface-attached colonies. Our results uncover a simple, yet hitherto overlooked, mechanical mechanism determining the outcome of bacterial competition, which is potentially ubiquitous among various bacteria. With the current advances in genetic engineering, varying aspect ratios can work as a simple tunable mechanism for the on-demand setting of the outcome of bacterial competitions with widespread implications for biofilm control.

RESULTS

Long bacteria win exclusively – even when outnumbered

We began by mixing two substrains of the non-motile *Escherichia coli* B: wild-type (WT) with a plasmid coding for green fluorescent protein (GFP) and an *mreB* mutant (AK) with a smaller aspect ratio (Table 1 and Supplementary Fig. S1) and with a plasmid coding for red fluorescent protein (RFP), see Fig. 1A. The mixture was inoculated on agar (1.5%) and resulted (after incubation) in a colony with three distinct regions from the centre and outwards (Fig. 1B): (i) the "homeland" where both strains were well mixed, (ii) a band thought to arise from the up-concentration of cells on the rim of the inoculation droplet (i.e., "coffee ring" (16, 17)), followed by (iii) a band where sectors merged. Strikingly, the WT (green) strain won over the shorter AK (magenta) during range expansion (outermost region of iii). We verified that these strains had similar growth rates (Supplementary Fig. S2A) and that takeover was independent of inoculation density (Supplementary Fig. S3). However, we found that the shorter strain had a growth advantage (in respect to the longer) in co-cultures (Supplementary Fig. S2B-C). Thus, WT wins in surface-attached colonies, even though this strain has a fitness disadvantage in liquid cultures.

To measure the strength of WT's advantage, we assessed the competition outcome for different strain ratios ζ, which we defined as the inoculation density of the longer strain versus the shorter, quantified by optical density (OD_{600}). We varied the ratio to identify the lower ζ-limit for WT to outcompete AK. However, for all tested strain ratios ζ (keeping combined inoculation density fixed), the longer strain (WT) consistently won over the shorter (AK) within the incubation time (20 h), see Fig. 1B. The takeover was noticeably slower in the $\zeta = 0.001$ case, where WT sectors (green) spread azimuthally while curving around cone-shaped regions of shorter bacteria (magenta). Due to the difference in cell volume (Table 1), the number of cells in the stationary phase with same OD_{600} value is ~ 1.3 times higher for WT than for AK (Materials and Methods). However,

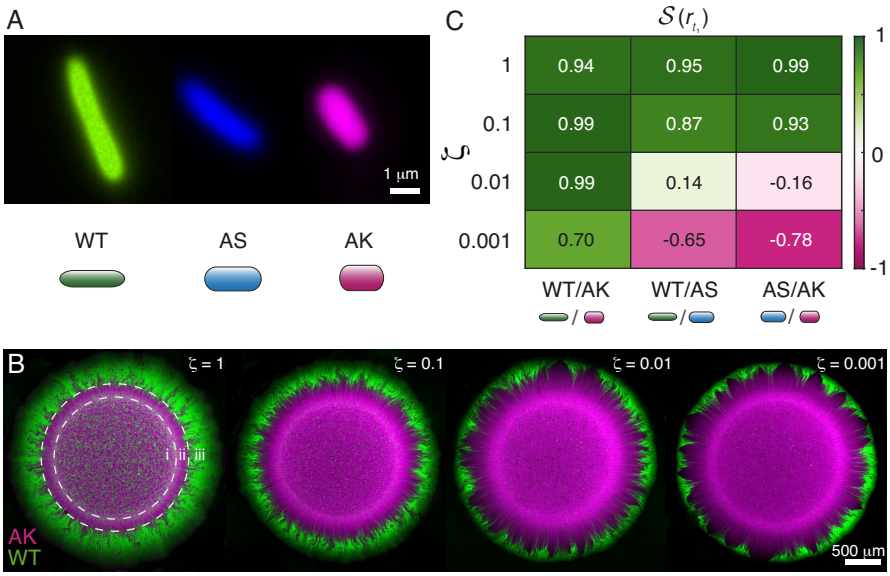

Figure 1: **Long bacteria win even when initially outnumbered.**
A: Single-cell (pseudo-coloured) fluorescence images of the wild type (WT) and the *mreB* mutants (AS and AK). The scale bar is 1 µm. **B:** Maximum-intensity projected (pseudo-coloured) confocal scanning laser microscopy images of 20 h competition experiments between WT (green) and AK (magenta) at different initial (WT/AK) ratios: $\zeta = \{1, 0.1, 0.01, 0.001\}$. Three distinct regions: (i) homeland, (ii) coffee ring, and (iii) a band where sectors merged. The scale bar is 500 µm. **C:** Heat map of strength, $\mathcal{S}(r_{t_1})$, at the specific radial distance r_{t_1} corresponding to the time: $t_1 = 1.5$ days and averaged over several colonies (Supplementary Fig. S4). $\mathcal{S} = 1$ corresponds to the longer cells (WT or AS) winning, $\mathcal{S} = -1$ to the shorter (AS or AK), and $\mathcal{S} = 0$ to equal strength (i.e., neutral fitness). The heat map shows all three strain combinations AS/AK, WT/AS, and WT/AK versus ζ. The cell graphics are to scale (Table 1).

because WT outcompetes AK even for the low strain ratios ($\zeta \ll 1$), this slight advantage (in numbers) of WT is not enough to explain the competition outcome. Together, these results showed that the longer WT bacteria outcompete the shorter AK strain, even when initially outnumbered.

To explore the robustness of the impact of the aspect ratio, we introduced an additional *mreB* mutant (AS) with an intermediate aspect ratio (Fig. 1A and Supplementary Fig. S2) and set up competition experiments over 3 days (Supplementary Fig. S4). We kept the colour-coding, such that longer cells expressed GFP (WT or AS) and shorter RFP (AS or AK), and found no systematic dependence on the colour (Supplementary Fig. S5). While the intermediate AS strain lost against the longer WT bacteria, this previously losing AS outcompeted the shorter AK strain. This indicates that the aspect ratio of individual bacteria is the determining factor for the competition outcome in dividing *E. coli*. To quantify the competitive strength, we segmented and filtered the image stacks to obtain 2D masks reconstituting a connected colony surface, where all pixels were assigned one and only one colour. Behind the expanding colony front, additional cell-layers are formed, so we investigated the cross-sections (Supplementary Fig. S6) to rule out any dramatic changes in the composition of cells along the vertical direction. On this mask, we defined the radial distance $r(t)$, from the homeland boundary (i.e., the ring of high intensity of shorter cells). Then, we measured the strength $\mathcal{S}(r)$, defined by the re-scaled occupancy of the longer cell, such that $\mathcal{S} = 1$ ($\mathcal{S} = -1$) signified that the longer (shorter) cells fully dominated. Fig. 1C is a heat map of how ζ controls the strength, $\mathcal{S}(r_{t_1})$, at the radial distance corresponding to the time point $t_1 = 1.5$ days of incubation (Materials and Methods). The quantitative analyses confirmed

Name	l (µm)	w (µm)	l/w	V_{cell} (µm^3)	V_{cell} (µm^3)*
WT	2.68 ± 0.45	0.68 ± 0.09	3.97 ± 0.14	0.88 ± 0.16	0.40 ± 0.06
AS	2.34 ± 0.34	0.99 ± 0.11	2.36 ± 0.08	1.54 ± 0.42	0.77 ± 0.47
AK	1.82 ± 0.30	1.05 ± 0.13	1.74 ± 0.07	1.27 ± 0.56	0.51 ± 0.26

Table 1: Length (l), width (w), aspect ratio (l/w), and cell volume (V_{cell}), in logarithmic phase. * denotes the average V_{cell} in stationary phase. All values are given as the mean ±SD (Supplementary Fig. S1).

that WT always wins over AK, even when initially outnumbered by as much as $\zeta = 0.001$ (i.e., one in thousands). For AS/AK and WT/AS combinations, we found few successful formations of sectors of the longer strain for $\zeta \leq 0.01$, indicating that the outcome is highly stochastic for small ζ (Supplementary Fig. S4); averaging over several colonies resulted in $\mathcal{S}(r_{t_1}) \lesssim 0$. However, the sectors with longer bacteria tended to spread azimuthally with increasing r, indicating that they are likely to win the expanding front later on. In other words, the strain of longer aspect ratio could take over, if they succeeded in forming sectors early on (i.e., at small r).

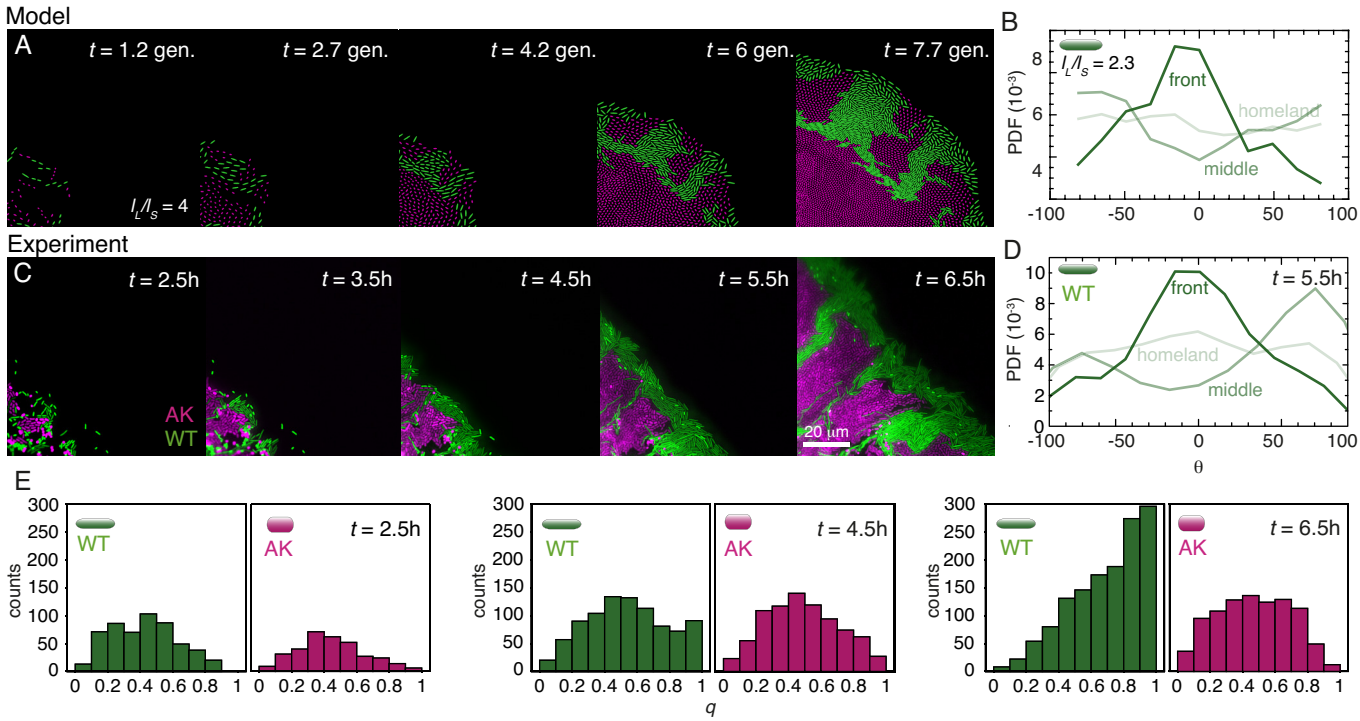

Figure 2: **Alignment-induced mechanism gives longer bacteria a mechanical winning advantage.**
A: Time series of particle-based simulations, where long bacteria (green) overtake the short bacteria (magenta) at the colony front by forming expanding regions along the front. The ratios between the aspect ratios were $l_L/l_S = 2.3$ ($\sim$ aspect ratio difference of WT and AK) and between the species: $\zeta_i = 0.25$. **B:** The probability distribution function, PDF, of the angle, θ, to the expansion front at three equidistant regions of r: the region were particles originally was deposited (homeland), closest to the outer rim (front), and the region in between (middle) at time: $t = 7.7$ gen. **C:** Snapshots from (pseudo-coloured) fluorescence time-lapses of competition between WT (green) and the *mreB* mutant AK (magenta) at time t after inoculation. The scale bar is 20 µm. **D:** The probability distribution function, PDF, of the angle, θ, to the expansion front at three equidistant regions of r: where the inoculation droplet originally was deposited (homeland), closest to the outer rim (front), and the region in between (middle). Data are from $t = 5.5$ hours in (C). **E:** The nematic order parameter, q, of the experimental data in (C) for WT and AK individually corresponding to every second time frame in (A) $t \in \{2.5, 4.5, 6.5\}$h. The distributions did not differ significantly after 2.5 h ($p > 0.1$) but they differed increasingly after 4.5 and 6.5 h ($p < 0.001$).

Alignment-induced mechanism gives longer bacteria a mechanical winning advantage

The experimental results suggested cell aspect ratio to be the determinant of the outcome of bacterial competition. In order to test if this is solely based on the mechanics of bacterial organisation, we simulated the range expansion in a minimal agent-based model (Materials and Methods). Bacteria were modelled as non-motile repulsive particles expanding on a 2D surface. The particles grew with the same fixed rate (with stochasticity). We distinguished longer from shorter species by setting the length at division as l_L and l_S, respectively. By using a constant width of $w = 1$, the aspect ratio (l/w) of these particles were l_L and l_S. We used an inoculation ratio, $\zeta_i = 0.25$ (ratio of number of long species over short), such that shorter bacteria were in majority, and placed individual particles (either $l_L = 8$ or $l_S = 3.5$) randomly in a small region. We then let the cells grow and interact to expand over the 2D surface, as seen in Fig. 2A.

As time evolved, the longer cells formed "channels" to the interface, in which they were aligned along the radial vector, **r**.

After the homeland had reached uniform density and the radial expansion began, longer cells squeezed through the channels to the colony front. As a result, the longer bacteria slowly began to dominate at the front, where they aligned with the interface. This channel-formation resulted in azimuthal spread of sectors of longer bacteria with increasing radial distance from the centre of the inoculation to the expanding front, r_f. Eventually, the sectors of longer bacteria curved around the sectors of shorter ones and took over the front. Thereby, the shorter cells lost their access to the front and, hence, nutrients and space. This suggests a purely mechanical mechanism. Longer bacteria locally form highly aligned domains (i.e., nematic arms), which connect the homeland to the outer rim of the colony and form a channel for longer bacteria to reach the front. Once at the front, the longer bacteria align parallel to it, as shown in Fig. 2B, and form a barrier, preventing further expansion of shorter bacteria (the case with short cell dividing faster is simulated for comparison (Supplementary Fig. S7)). Importantly, while the only difference between the competing bacteria in the model is their aspect ratio, this winning mechanism is an emergent collective property of bacteria that are longer than their neighbours.

To test the mechanism suggested by the cell-based model and investigate how populations compete at the individual cell scale, we ran time-lapse experiments with single-cell resolution. *E. coli* colonies were inoculated from a suspension of WT/AK in equal proportions ($\zeta = 1$). We imaged the growth at the colony front over time t, as shown in Fig. 2C (Movie 1) and for an additional time-lapse (Supplementary Fig. S8, Movie 2). Individual bacteria were segmented and their orientation was determined and the angle, θ, to the expanding colony front (i.e., 90° to $\mathbf{r}$) in three equidistant regions of r was measured (Fig. 2D). In agreement with the alignment-induced mechanical mechanism suggested by the agent-based model, we found that the winning WT bacteria align along $\mathbf{r}$ (inside the colony) or along the expanding colony front. Furthermore, the nematic order parameter, q, which is a measurement of local orientation alignment (18), was calculated for every bacterium relative to its 8 closest neighbours, as extensively reported for bacterial mono-cultures (8, 19–23). The distribution of q was analysed at three different time points: $t \in \{2.5, 4.5, 6.5\}$ h in Fig. 2E. The distributions of WT and AK strains did not differ significantly after 2.5 h ($p > 0.1$), but they differed increasingly after 4.5 and 6.5 h ($p < 0.001$). The distributions account for the visual observations in Fig. 2C that WT cells align with each other, while AK's alignment was weak. Together, model predictions and experimental quantifications show how the longer WT are squeezed by small clusters of growing AK cells and form channels of (radially) aligned bacteria. When they reach the colony front, they align with the expanding front and start dividing along the tangential direction. In this way, WT cut their shorter AK counterparts off from both nutrients and space.

To emphasise the generic mechanical nature of this takeover mechanism – set by aspect ratio and enhanced by stronger local alignment – we also employed a continuum model of a bi-phasic active nematic, where we took the two different bacteria types into account with an additional phase field order parameter ϕ, where $\phi > 0$ ($\phi < 0$) corresponded to longer (shorter) bacteria regions modelled with a higher (lower) elastic constant and extensile activity (which mimics the dipolar force of division (24, 25)). It is well established that both orientational elasticity and extensile division activity are higher for higher aspect ratios (26, 27). We observed that even when the front is mostly populated by shorter bacteria, the phase corresponding to the more elongated bacteria eventually overtakes the shorter (Supplementary Fig. S9). Importantly, this phase segregation is solely driven by activity, stemming from cell divisions, and differences between aspect ratios, without any free-energy-driven phase separation. Remarkably, the longer bacteria take over the front by forming perpendicularly aligned nematic channels to the interface, in agreement with both the cell-based model and experimental observations (Fig. 2A and 2C). Consequently, the longer bacteria spread at the interface, as they aligned more strongly with it, due to their higher elastic constant.

Takeover rate is set by differences in aspect ratios and the length of the shorter cell

Having established the competitive advantage of a large aspect ratio through experimental observations, cell-based and continuum models, we next turned to investigating the takeover rates. Fig. 3A shows the experimentally obtained strength $\mathcal{S}(r)$ from the homeland ($r = 0$) to the outer rim of the colonies for the strain combinations and ζ-values that clearly switched within 3 days (i.e., $\mathcal{S}(r_{t_1}) > 0.85$ in Fig. 1C). We defined the takeover rates, ν, as the slope of $\mathcal{S}(r)$ and summarised them in Fig. 3B versus the length of the shorter strain (i.e., l_S). We paralleled this result with the agent-based simulations to measure the time-dependent strength, $\mathcal{S}(r_f(t))$ (Fig. 3C) and the associated takeover rate, $\nu_{\text{sim.}}$. This rate was also dependent on the aspect ratio difference l_L/l_S, as a more significant l_L/l_S resulted in a stronger alignment along the channels (Supplementary Fig. S10). Hence, the longer bacteria had enhanced access to the colony front. This is in agreement with the experimental observation that ν is larger for WT/AK than WT/AS.

Surprisingly, we found that the takeover rates for the competition between longest and intermediate strains, WT/AS (grey), are significantly slower than for the two other strain combinations (longest versus shortest, WT/AK, and intermediate versus shortest, AS/AK), although the ratios of aspect ratios (Table 1) were similar for WT/AS and AS/AK (~ 1.5). Since our results established that the alignment-induced mechanism governs the competition between growing bacteria, we hypothesised that the difference in takeover rates were related to the relative ability of bacteria to form nematic domains. To explain the differences in the takeover rate ν between WT/AS (longest versus intermediate) and AS/AK (intermediate versus shortest) (Fig. 3B),

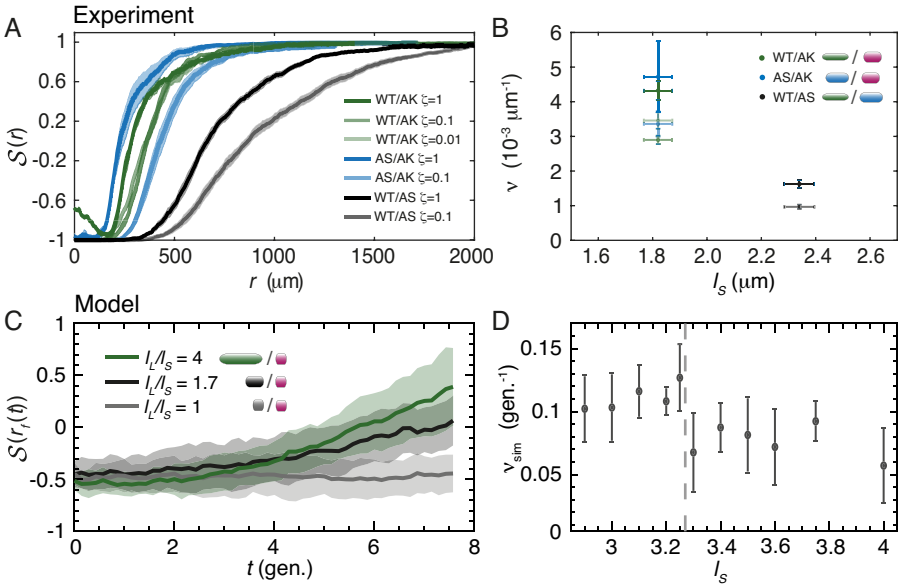

Figure 3: **Takeover rate is set by differences in aspect ratios and the length of the shorter cell.**
A: Competition is evaluated by the strength, $\mathcal{S}(r)$, along the radial length, r, for the strain and ratios, ζ, and strain combinations WT/AK (green), AS/AK (blue), and WT/AS (grey). We collected data from $N \in \{5, 4, 5, 6, 8, 9, 9\}$ colonies (following order of legend) and ran the experiments for 3 days for all colonies to switch completely from -1 to $+1$, which was the case for strain combinations and ζ-values that fulfilled $\mathcal{S}(r_{t_1}) > 0.85$ in Fig. 1C. Notice how WT/AK mixed $\zeta = 1$ drops from a higher $\mathcal{S}$-level at the homeland boundary ($r = 0$) before switching again. The shaded regions correspond to ±SEM. **B:** Takeover rate, ν, from (A) for WT/AK (green), AS/AK (blue), and WT/AS (grey) versus length of the shorter cell, l_S, for varying ζ (opacity as legend in (A)). Slopes are found for the individual colonies by fitting the linear part around $\mathcal{S} \sim 0$ and ν is the ensemble-average over $N \in \{5, 4, 5, 6, 8, 9, 9\}$ colonies (following order of legend in (A)). The error bars correspond to ±SEM. ν of WT/AS ($\zeta = 1$) is significantly different from AS/AK ($p < 0.01$) and WT/AK ($p << 0.001$). **C:** The time evolution of strength at the front, $\mathcal{S}(r_f(t))$, where $r_f(t)$ is the radial distance from the centre of the inoculation to the expanding front at time, t. The long bacteria cell aspect ratio is fixed to $l/w = 4$, the species ratio is set to $\zeta_i = 0.25$, and $l_L/l_S = 4, 1.7$, and 1 are shown. The shaded regions correspond to ±SEM and $N = 10$. **D:** The simulation takeover rate, $\nu_{\text{sim.}}$, (slope of (C) between $t = 30$ gen. to $t = 45$ gen.) for varying lengths of the shorter bacteria, l_S, with fixed ratio between long and short bacteria: $l_L/l_S = 1.5$. In simulations, bacteria with $l_S \leq 3.25$ (dashed vertical line) are dominantly isotropic and bacteria with larger l_S are dominantly nematic. The error bars correspond to ±SEM and $N = 10$.

we used the agent-based model to examine the takeover rate for fixed l_L/l_S ratio (~1.5), while varying l_S from no local alignment (isotropic) to local alignment (nematic). The transition between isotropic and nematic states is set by excluded volume interactions and is dictated by local density and particle length (28). Given our simulation doubling time, this transition occurred at around length $l_S = 3.25$. The agent-based model showed that the takeover rate dropped when both bacteria strains had local orientation ordering, see Fig. 3D. This explains why the switching speed was slower for WT/AS than for AS/AK: WT and AS both had nematic order, while in the AS/AK strain combination, only the longer AS were nematically aligning. This is also in accordance with the observation that the sector boundaries are more rugged for WT/AS (Supplementary Fig. S4), indicating that AS cells might be weakly aligning. Together, these results further highlight the emergent alignment as enhancing the takeover strength of the competing surface-attached bacteria and the importance of isotropic or nematic state of bacteria groups. The takeover rate is independent of the length of the individual bacteria, but only when the orientational packing of the mono-culture is the same (i.e. both species are within the isotropic or nematic phases). When, due to their individual lengths, the shortest bacteria species transition from isotropically packed to nematically ordered state, the takeover rate changes.

Competition strength weakens in 3D

After establishing the significant advantage of elongation for surface-attached cells, we turned to 3D growth. The results so far have established that emergent nematic alignment is a competitive advantage. The local nematic order has been observed in 3D biofilms (29), though theoretically, it is expected that the nematic alignment weakens in 3D (30, 31) and as such we expected

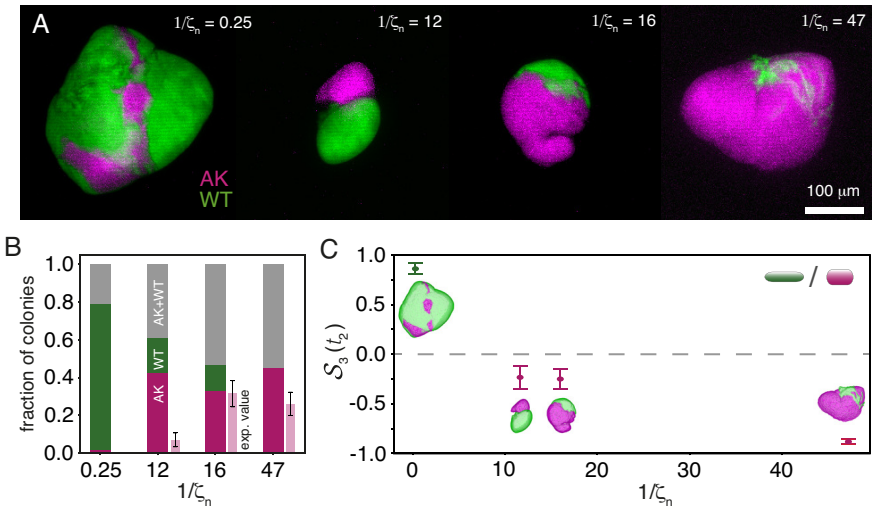

Figure 4: **Competition strength weakens in 3D colonies compared to surface-attached bacteria.**
A: Maximum-intensity projected (pseudo-coloured) fluorescence images of colonies formed from WT/AK inoculation beads of different ratios, ζ_n. The scale bar corresponds to 100 µm. **B:** Fraction of colonies with mono-coloured surfaces (WT or AK) or both (WT+AK). Predicted number of colonies (exp. value) originating from pure AK inoculation beads. Error bars correspond to ±SD. **C:** Strength, $\mathcal{S}_3(t_2)$, of the ensemble of colonies versus $1/\zeta_n$, measured in (A). Here 1 (−1) corresponds to the longer (shorter) cells winning within the time, t_2 = 10 h, and 0 to equal strength (dashed grey line). The error bars correspond to ±SEM and the number of colonies were $N \in \{52, 49, 45, 53\}$ for $1/\zeta_n \in \{0.25, 12, 16, 47\}$, respectively.

that the takeover strength weakens, compared to surface-attached (2D) conditions. We tested our predictions in WT/AK colonies grown from inoculation beads of small volume (0.05 nl) in low-density (0.5%) agar (inset of Supplementary Fig. S11). We defined a strain ratio, ζ_n, as the ratio of colony-forming units (CFU) of the longer strain versus the shorter (Supplementary Fig. S11), and imaged (with confocal-scanning laser microscopy) the resulting 3D colonies for various ζ_n, as shown in Fig. 4A. We then sorted the ensemble of colonies into subgroups of either mono-coloured colonies (WT or AK) or colonies with both strains surviving at the surface (grey); distributions are given in Fig. 4B. For comparison, we also calculated (assuming a binomial distribution) the fraction of colonies that initially contained only AK or WT. The probability of a pure WT inoculation was negligibly small in all cases, in contrast to the probability of pure AK. It is, thus, unlikely that all mono-coloured WT colonies arose from pure WT inoculation beads. Instead, the longer strain (WT) had outcompeted the shorter (AK) during range expansion. We also found examples of the inverse, where AK had taken over the colony surface, even though the inoculum had both WT and AK.

To quantify the takeover strength, we segmented and filtered the image stacks to obtain 3D masks reconstituting a connected colony surface with the width of a single voxel, which were assigned one and only one colour (Supplementary Fig. S12 and Movie 3). In order to determine the strength, $\mathcal{S}_3(t_2)$, at a specific time, t_2, we quantified the proportion of the WT strain on the colony surface, as found in Fig. 4C. Interestingly, we found that when WT/AK are mixed four to one (i.e., $1/\zeta_n = 0.25$) WT occupies > 90% of the surface and that $\mathcal{S}_3(t_2)$ decreases, as $1/\zeta_n$ increases. However, the longer (WT) still occupies a significant fraction despite a low initial ratio in the inoculation beads (Supplementary Fig. S12). For instance, when WT is only ∼ 2% of the inoculations ($1/\zeta_n = 47$), it still occupies ∼ 6% of the final colonies' surfaces. Taken together, our results indicate that the longer cell still wins, but that its competitive strength is weakened.

DISCUSSION

Using a set of three non-motile *E. coli* substrains, differing only in cell aspect ratios, we revealed that longer bacteria outcompete their shorter counterparts, even when initially outnumbered. By simulating the 2D colony growth, using the agent-based model of growing elongated particles with repulsive interactions, we showed that the advantage originates from local nematic ordering induced by mechanical interactions. The finding was experimentally confirmed by time-lapses of the takeover process at single-cell resolution: The longer WT cells aligned and formed nematic channels linking the homeland to the expanding front. After this, they aligned perpendicular to the front and eventually surrounded the whole colony, while the shorter AK cells were

cut off from nutrients and space. We further confirmed that this advantage is reproduced in 3D colonies, even though the effect was less prominent than in surface environments. We also found (from mono-strain colonies) that WT expands faster over a substrate surface than the shorter mutants (Supplementary Fig. S13), whose slower radial expansion is compensated by an increase in thickness (32–34). As the takeover happens in the monolayer at the expanding front, the expansion rate is not the determinant of the competition, instead it is the strain-strain interaction – enhanced by local alignment.

It has been long argued, based on phylogenetic studies, that the morphological development from rod-shaped to round-shaped bacteria (cocci) has happened independently several times and is associated with the loss of *mreB* (35–37). In long-term evolutionary experiments (in liquid medium), an *E. coli* B strain was found to enlarge its volume by shortening and widening (38, 39) in favour of enhanced metabolic efficiency (40). However, our results suggest that in other natural habitats such as on surfaces, in soils, and animal tissue, which are typically associated with spatial constraints and unpredictable supplies of nutrients, the advantageous morphology is the rod-shape, which conquers the habitat due to the enhanced ability of forming orientationally ordered domains extending from the homeland to the expansion front.

It is well-understood that morphology shapes colonies (e.g., tortuosity of sector boundaries (Supplementary Fig. S14-S15) (41, 42), swarming efficiency (43) and layering (44)). However, our results highlight an additional, yet so far overlooked, emergent property of bacteria in large communities caused by generic mechanical interactions rather than species-specific chemical cues. The simplicity of this morphological feature suggests a potential to be generalised over a wide range of bacteria species, confirmed by the reproduction of the results using minimal mechanical agent-based model and a generic continuum model. Our findings show how generic bacterial aspect ratios can influence bacterial advancements in growing colonies. Since biofilm-formation impacts various human activities (45, 46), a better understanding of their mechanical determinants can benefit numerous sectors, including ground remediation, biofouling of industrial installations, and changes in human microbiomes. The mechanical advantage of larger aspect ratios uncovered in this manuscript allows for a generic pathway to control biofilms by modifying the length of various bacteria, which is already achievable with existing technologies (47–49).

AUTHOR CONTRIBUTIONS

NM and LJ conceived the original idea. NvdB, AS, and TTN conducted the experimental research including analysis. Specifically, NvdB did the surface-attached colony investigations, AS the single-cell resolved investigations, and TTN the 3D investigations. AD conceived the cell-based and continuum models. KT did the cell-based and continuum modelling. MC and AGV co-supervised the project and conducted substantial control experiments. NM, AD, and LJ supervised the project.

FUNDING

This work was supported by the Danish National Research Foundation grant no. DFF 0165-00032B and grant no. DFF 0165-00103B (LJ), the Novo Nordisk Foundation grant no. NNF18SA0035142, NERD grant no. NNF21OC0068687 (AD) and grant no. NNF21OC0068775 (NM) and Synergy grant no. NNF23OC0086712 (LJ), the Villum Fonden Grant no. 29476 (AD), and the European Union via the ERC-Starting Grant PhysCoMeT (AD) and the Horizon 2020 research and innovation programme Marie Sklodowska-Curie grant no. 101029079-SIMMS (KT).

ACKNOWLEDGEMENTS

The authors thank Dr. Michael Lisby for access to the FACS instrument and for generously sharing his expertise.

REFERENCES

1. Flemming, H.-C., and S. Wuertz, 2019. Bacteria and archaea on Earth and their abundance in biofilms. Nature Reviews Microbiology 17:247–260. https://www.nature.com/articles/s41579-019-0158-9.

2. Ghoul, M., and S. Mitri, 2016. The Ecology and Evolution of Microbial Competition. Trends in Microbiology 24:833–845. https://linkinghub.elsevier.com/retrieve/pii/S0966842X16300749.

3. Nadell, C. D., K. Drescher, and K. R. Foster, 2016. Spatial structure, cooperation and competition in biofilms. Nature Reviews Microbiology 14:589–600. https://doi.org/10.1038/nrmicro.2016.84.

4. Persat, A., C. Nadell, M. Kim, F. Ingremeau, A. Siryaporn, K. Drescher, N. Wingreen, B. Bassler, Z. Gitai, and H. Stone, 2015. The Mechanical World of Bacteria. Cell 161:988–997. https://linkinghub.elsevier.com/retrieve/pii/S0092867415005528.

5. Raffatellu, M., 2018. Learning from bacterial competition in the host to develop antimicrobials. Nature Medicine 24:1097–1103. https://www.nature.com/articles/s41591-018-0145-0.

6. Piccardi, P., B. Vessman, and S. Mitri, 2019. Toxicity drives facilitation between 4 bacterial species. Proceedings of the National Academy of Sciences 116:15979–15984. https://pnas.org/doi/full/10.1073/pnas.1906172116.

7. Rakoff-Nahoum, S., K. R. Foster, and L. E. Comstock, 2016. The evolution of cooperation within the gut microbiota. Nature 533:255–259. http://www.nature.com/doifinder/10.1038/nature17626.

8. Meacock, O. J., A. Doostmohammadi, K. R. Foster, J. M. Yeomans, and W. M. Durham, 2021. Bacteria solve the problem of crowding by moving slowly. Nature Physics 17:205–210. http://dx.doi.org/10.1038/s41567-020-01070-6https://www.nature.com/articles/s41567-020-01070-6.

9. Lee, H., J. Gore, and K. S. Korolev, 2022. Slow expanders invade by forming dented fronts in microbial colonies. Proceedings of the National Academy of Sciences 119:e2108653119. https://pnas.org/doi/full/10.1073/pnas.2108653119.

10. Gude, S., E. Pinçe, K. M. Taute, A.-B. Seinen, T. S. Shimizu, and S. J. Tans, 2020. Bacterial coexistence driven by motility and spatial competition. Nature 578:588–592. http://dx.doi.org/10.1038/s41586-020-2033-2https://www.nature.com/articles/s41586-020-2033-2.

11. Cordero, M., N. Mitarai, and L. Jauffred, 2023. Motility mediates satellite formation in confined biofilms. The ISME Journal 17:1819–1827. https://www.nature.com/articles/s41396-023-01494-x.

12. Booth, S. C., W. P. J. Smith, and K. R. Foster, 2022. Bows and swords : why bacteria carry short and long-range weapons. bioRxiv https://www.biorxiv.org/content/10.1101/2022.10.13.512033v1.

13. Borenstein, D. B., P. Ringel, M. Basler, and N. S. Wingreen, 2015. Established Microbial Colonies Can Survive Type VI Secretion Assault. PLOS Computational Biology 11:e1004520. https://dx.plos.org/10.1371/journal.pcbi.1004520.

14. Hallatschek, O., P. Hersen, S. Ramanathan, and D. R. Nelson, 2007. Genetic drift at expanding frontiers promotes gene segregation. Proceedings of the National Academy of Sciences 104:19926–19930. https://pnas.org/doi/full/10.1073/pnas.0710150104.

15. Vázquez, A. G., N. Mitarai, and L. Jauffred, 2024. Genetic mixing and demixing on expanding spherical frontiers. ISME Communications https://academic.oup.com/ismecommun/advance-article/doi/10.1093/ismeco/ycae009/7585292.

16. Deegan, R. D., O. Bakajin, T. F. Dupont, G. Huber, S. R. Nagel, and T. A. Witten, 1997. Capillary flow as the cause of ring stains from dried liquid drops. Nature 389:827–829. https://www.nature.com/articles/39827https://doi.org/10.1038/39827.

17. Ruan, C., B. Borer, J. Ramoneda, G. Wang, and D. R. Johnson, 2023. Evaporation-induced hydrodynamics control plasmid transfer during surface-associated microbial growth. Biofilms and Microbiomes 9:58. https://www.nature.com/articles/s41522-023-00428-x.

18. De Gennes, P.-G., and J. Prost, 1993. The physics of liquid crystals. 83. Oxford university press.

19. Dhar, J., A. L. P. Thai, A. Ghoshal, L. Giomi, and A. Sengupta, 2022. Self-regulation of phenotypic noise synchronizes emergent organization and active transport in confluent microbial environments. Nature Physics 18:945–951. https://www.nature.com/articles/s41567-022-01641-9.

20. You, Z., D. J. Pearce, A. Sengupta, and L. Giomi, 2018. Geometry and Mechanics of Microdomains in Growing Bacterial Colonies. Physical Review X 8:031065. https://link.aps.org/doi/10.1103/PhysRevX.8.031065.

21. Nijjer, J., C. Li, M. Kothari, T. Henzel, Q. Zhang, J.-S. B. Tai, S. Zhou, T. Cohen, S. Zhang, and J. Yan, 2023. Biofilms as self-shaping growing nematics. Nature Physics 19:1936–1944. https://www.nature.com/articles/s41567-023-02221-1.

22. Hartmann, R., P. K. Singh, P. Pearce, R. Mok, B. Song, F. Díaz-Pascual, J. Dunkel, and K. Drescher, 2019. Emergence of three-dimensional order and structure in growing biofilms. Nature Physics 15:251–256. https://www.nature.com/articles/s41567-018-0356-9.

23. Copenhagen, K., R. Alert, N. S. Wingreen, and J. W. Shaevitz, 2021. Topological defects promote layer formation in Myxococcus xanthus colonies. Nature Physics 17:211–215. https://www.nature.com/articles/s41567-020-01056-4.

24. Allen, R. J., and B. Waclaw, 2019. Bacterial growth: a statistical physicist's guide. Reports on Progress in Physics 82:016601. https://iopscience.iop.org/article/10.1088/1361-6633/aae546.

25. Doostmohammadi, A., S. P. Thampi, and J. M. Yeomans, 2016. Defect-Mediated Morphologies in Growing Cell Colonies. Physical Review Letters 117:048102. https://link.aps.org/doi/10.1103/PhysRevLett.117.048102.

26. Wittmann, R., G. H. P. Nguyen, H. Löwen, F. J. Schwarzendahl, and A. Sengupta, 2023. Collective mechano-response dynamically tunes cell-size distributions in growing bacterial colonies. Communications Physics 6:331. https://www.nature.com/articles/s42005-023-01449-w.

27. Kröger, M., and P. Ilg, 2007. Derivation of Frank-Ericksen elastic coefficients for polydomain nematics from mean-field molecular theory for anisotropic particles. The Journal of Chemical Physics 127. https://pubs.aip.org/jcp/article/127/3/034903/904677/Derivation-of-Frank-Ericksen-elastic-coefficients.

28. Speranza, A., and P. Sollich, 2002. Simplified Onsager theory for isotropic-nematic phase equilibria of length polydisperse hard rods. The Journal of Chemical Physics 117:5421–5436. https://pubs.aip.org/jcp/article/117/11/5421/184912/Simplified-Onsager-theory-for-isotropic-nematic.

29. Drescher, K., J. Dunkel, C. D. Nadell, S. van Teeffelen, I. Grnja, N. S. Wingreen, H. A. Stone, and B. L. Bassler, 2016. Architectural transitions in Vibrio cholerae biofilms at single-cell resolution. Proceedings of the National Academy of Sciences 113. https://pnas.org/doi/full/10.1073/pnas.1601702113.

30. Tan, X., Y. Chen, H. Wang, Z. Zhang, and X. S. Ling, 2021. 2D isotropic-nematic transition in colloidal suspensions of ellipsoids. Soft Matter 17:6001–6005. http://xlink.rsc.org/?DOI=D1SM00367D.

31. Roller, J., J. D. Geiger, M. Voggenreiter, J.-M. Meijer, and A. Zumbusch, 2020. Formation of nematic order in 3D systems of hard colloidal ellipsoids. Soft Matter 16:1021–1028. http://xlink.rsc.org/?DOI=C9SM01926J.

32. Su, P.-T., C.-T. Liao, J.-R. Roan, S.-H. Wang, A. Chiou, and W.-J. Syu, 2012. Bacterial Colony from Two-Dimensional Division to Three-Dimensional Development. PLoS ONE 7:e48098. https://dx.plos.org/10.1371/journal.pone.0048098.

33. Duvernoy, M.-C., T. Mora, M. Ardré, V. Croquette, D. Bensimon, C. Quilliet, J.-M. Ghigo, M. Balland, C. Beloin, S. Lecuyer, and N. Desprat, 2018. Asymmetric adhesion of rod-shaped bacteria controls microcolony morphogenesis. Nature Communications 9:1120. https://www.nature.com/articles/s41467-018-03446-y.

34. Steinberger, R., A. Allen, H. Hansma, and P. Holden, 2002. Elongation Correlates with Nutrient Deprivation in Pseudomonas aeruginosa Unsaturated Biofilms. Microbial Ecology 43:416–423. http://link.springer.com/10.1007/s00248-001-1063-z.

35. Yulo, P. R. J., and H. L. Hendrickson, 2019. The evolution of spherical cell shape; progress and perspective. Biochemical Society Transactions 47:1621–1634. https://portlandpress.com/biochemsoctrans/article/47/6/1621/221467/The-evolution-of-spherical-cell-shape-progress-and.

36. Errington, J., 2013. L-form bacteria, cell walls and the origins of life. Open Biology 3:120143. https://royalsocietypublishing.org/doi/10.1098/rsob.120143.

37. Siefert't, J. L., and G. E. Fox, 1998. Phylogenetic mapping of bacterial morphology. Microbiology 144:2803–2808. https://www.microbiologyresearch.org/content/journal/micro/10.1099/00221287-144-10-2803.

38. Lenski, R. E., M. R. Rose, S. C. Simpson, and S. C. Tadler, 1991. Long-Term Experimental Evolution in Escherichia coli. I. Adaptation and Divergence During 2,000 Generations. The American Naturalist 138:1315–1341. https://www.jstor.org/stable/2462549.

39. Grant, N. A., A. Abdel Magid, J. Franklin, Y. Dufour, and R. E. Lenski, 2021. Changes in Cell Size and Shape during 50,000 Generations of Experimental Evolution with Escherichia coli. Journal of Bacteriology 203. https://journals.asm.org/doi/10.1128/JB.00469-20.

40. Marshall, D. J., M. Malerba, T. Lines, A. L. Sezmis, C. M. Hasan, R. E. Lenski, and M. J. McDonald, 2022. Long-term experimental evolution decouples size and production costs in Escherichia coli. Proceedings of the National Academy of Sciences 119. https://pnas.org/doi/full/10.1073/pnas.2200713119.

41. Müller, M. J. I., B. I. Neugeboren, D. R. Nelson, and A. W. Murray, 2014. Genetic drift opposes mutualism during spatial population expansion. Proceedings of the National Academy of Sciences 111:1037–1042. https://pnas.org/doi/full/10.1073/pnas.1313285111.

42. Hallatschek, O., and D. R. Nelson, 2010. Life at the front of an expanding population. Evolution 64:193–206. https://academic.oup.com/evolut/article/64/1/193/6854125.

43. Ilkanaiv, B., D. B. Kearns, G. Ariel, and A. BeâĂŹer, 2017. Effect of Cell Aspect Ratio on Swarming Bacteria. Physical Review Letters 118:158002. http://link.aps.org/doi/10.1103/PhysRevLett.118.158002.

44. Smith, W. P. J., Y. Davit, J. M. Osborne, W. D. Kim, K. R. Foster, and J. M. Pitt-Francis, 2017. Cell morphology drives spatial patterning in microbial communities. Proceedings of the National Academy of Sciences 114:E280–E286. http://www.pnas.org/lookup/doi/10.1073/pnas.1613007114https://doi.org/10.1073/pnas.1613007114.

45. Shineh, G., M. Mobaraki, M. J. Perves Bappy, and D. K. Mills, 2023. Biofilm Formation, and Related Impacts on Healthcare, Food Processing and Packaging, Industrial Manufacturing, Marine Industries, and Sanitation-A Review. Applied Microbiology 3:629–665. https://www.mdpi.com/2673-8007/3/3/44.

46. Hayta, E. N., M. J. Ertelt, M. Kretschmer, and O. Lieleg, 2021. Bacterial Materials: Applications of Natural and Modified Biofilms. Advanced Materials Interfaces 8:2101024. https://onlinelibrary.wiley.com/doi/10.1002/admi.202101024.

47. Tanniche, I., and B. Behkam, 2023. Engineered live bacteria as disease detection and diagnosis tools. Journal of Biological Engineering 17:65. https://jbioleng.biomedcentral.com/articles/10.1186/s13036-023-00379-z.

48. Riglar, D. T., and P. A. Silver, 2018. Engineering bacteria for diagnostic and therapeutic applications. Nature Reviews Microbiology 16:214–225. https://www.nature.com/articles/nrmicro.2017.172.

49. Landry, B. P., and J. J. Tabor, 2017. Engineering Diagnostic and Therapeutic Gut Bacteria. Microbiology Spectrum 5. https://journals.asm.org/doi/10.1128/microbiolspec.BAD-0020-2017.